July 1998 ● NREL/CP-520-23874

1-eV GaInNAs Solar Cells for Ultrahigh-Efficiency Multijunction Devices

D.J. Friedman, J.F. Geisz, S.R. Kurtz, and J.M. Olson

Presented at the 2nd World Conference and Exhibition on
Photovoltaic Solar Energy Conversion; 6-10 July 1998; Vienna, Austria

National Renewable Energy Laboratory
1617 Cole Boulevard
Golden, Colorado 80401-3393
A national laboratory of the
U.S. Department of Energy
Managed by the Midwest Research Institute
For the U.S. Department of Energy
Under Contract No. DE-AC36-83CH10093

1-eV GaInNAs SOLAR CELLS FOR ULTRAHIGH-EFFICIENCY MULTIJUNCTION DEVICES

D. J. Friedman, J. F. Geisz, S. R. Kurtz, and J. M. Olson
National Renewable Energy Laboratory, 1617 Cole Blvd., Golden, CO 80401 USA

ABSTRACT: We demonstrate working prototypes of a GaInNAs-based solar cell lattice-matched to GaAs with photoresponse down to 1 eV. This device is intended for use as the third junction of future-generation ultrahigh-efficiency three- and four-junction devices. Under the AM1.5 direct spectrum with all the light higher in energy than the GaAs band gap filtered out, the prototypes have open-circuit voltages ranging from 0.35 to 0.44 V, short-circuit currents of 1.8 mA/cm^2, and fill factors from 61% to 66%. The short-circuit currents are of principal concern: the internal quantum efficiencies rise only to about 0.2. We discuss the short diffusion lengths which are the reason for this low photocurrent. As a partial workaround for the poor diffusion lengths, we demonstrate a depletion-width-enhanced variation of one of the prototype devices that trades off decreased voltage for increased photocurrent, with a short-circuit current of 6.5 mA/cm^2 and an open-circuit voltage of 0.29 V.
Keywords: GaInNAs - 1: Multijunction Solar Cells - 2: High-Efficiency - 3

1. INTRODUCTION

The $Ga_{0.5}In_{0.5}P$/GaAs tandem solar cell is in production for space photovoltaic applications and is a leading candidate for terrestrial high-concentration photovoltaics because of its record-setting efficiency [1-4]. The addition of an active Ge junction, yielding a three-junction device, has been demonstrated to boost efficiencies further [5]. However, the Ge band gap is not optimal for the third junction: significantly higher efficiencies would be obtained if the third junction could be fabricated from a 1-eV-band-gap material [6]. If this next generation of multijunction devices could be achieved, the Ge junction could be reintroduced under this three-junction stack for a resulting monolithic, two-terminal device with projected real-world efficiencies above 35% for air-mass 0 (AM0) and above 40% for 500-suns terrestrial [6]. This evolution of multijunction solar-cell structures from the existing two-junction device [1] to future-generation three- and four-junction devices is shown in Fig. 1. Projected idealized efficiencies [6] for these devices are summarized in Table I. (Practical efficiencies can be expected to be ~80% of the idealized values.) The crucial step in the evolution to these next generations of ultrahigh-efficiency devices is to develop the 1-eV third cell lattice-matched to GaAs (or Ge).

It has recently been shown that N induces a very large band-gap bowing for the $Ga_{1-x}In_xN_yAs_{1-y}$ alloy system. Concentrations of N as low as a few percent lower the band gap by a significant fraction of an eV [7]. Furthermore, with $y \approx 0.35x$, the alloy is lattice-matched to GaAs (or Ge). For these reasons, Kondow proposed and demonstrated this material as the active layer for a 1-eV laser [8]. Here, we propose this material for a 1-eV GaAs-lattice-matched solar cell. We demonstrate several working prototype 1-eV solar cells based on GaInNAs active layers lattice-matched to GaAs which may be suitable for the third cell of the next generations of ultrahigh-efficiency devices, if problems with

Table I. Projected idealized solar photovoltaic conversion efficiencies at 300K for the device structures of Fig. 1 [6]. The AM0 numbers apply to use in space, and the AM1.5D 500 suns numbers apply to use in terrestrial concentrator systems.

Device	AM0 1 sun	AM1.5D 500 suns
2 junction	31%	36%
3 junction (with Ge)	35%	42%
3 junction (with 1-eV)	38%	47%
4 junction	41%	52%

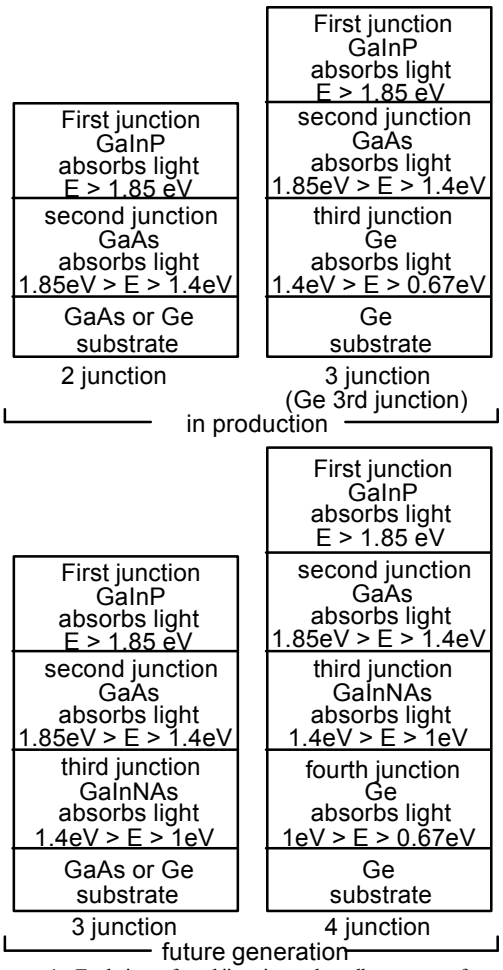

Figure 1. Evolution of multijunction solar-cell structures from the existing GaInP/GaAs two-junction device to three- and four- junction future-generation devices incorporating a 1-eV third junction. In each multijunction device, the individual cells are interconnected by tunnel junctions (not shown).

the quantum efficiency can be overcome.

2. DEVICE FABRICATION

The devices were grown by low-pressure metalorganic vapor-phase epitaxy on GaAs substrates oriented 2° to $(111)_B$ from (100), using trimethylgallium (TMGa), trimethylindium (TMIn), arsine (AsH_3), phosphine (PH_3), and dimethylhydrazine (DMHy) as the nitrogen source. For GaInNAs layers grown without any intentionally introduced dopant, the resulting background doping is *p*-type on the order of $10^{17}/cm^3$, probably largely from carbon introduced into the as-grown material from the dimethylhydrazine. Si (from disilane) and Se (from hydrogen selenide) were used as *n*-type dopants for the various layers, including the *n*-GaInNAs layers. Zn (from diethylzinc) was used as a *p*-type dopant for the GaAs and GaInP layers and for some of the GaInNAs layers. For other *p*-GaInNAs layers, the background *p*-type doping was used.

The nitrogen incorporation into GaInNAs is found to depend sensitively on the growth temperature and DMHy/AsH_3 flow ratio [9]; high temperatures lead to minimal incorporation, presumably because under these conditions growth proceeds near thermodynamic equilibrium, for which the N solubility is expected to be very small. For this reason, the GaInNAs layers of the devices presented here were grown at a relatively low temperature of ~580°–600°C, at a rate of 2.4 µm/hr and DMHy/AsH_3 flow ratio of 20. The compositions of the GaInNAs epilayers were determined by growing reference GaInNAs/GaAs structures under the same growth conditions as the GaInNAs layers in the devices, and then determining the compositions of the reference epilayers from x-ray diffraction measurements of the epilayer lattice constants [10]. The N concentrations were selectively cross-checked with secondary-ion mass spectroscopy (SIMS). The band gaps of the GaInNAs layers in the devices were determined from the device quantum efficiency (QE) curves, as discussed below.

The structures of the various prototype solar cells include both p/n and n/p GaInNAs homojunctions and a GaAs/GaInNAs heterojunction. The structures are shown schematically in Fig. 2. All the device structures include a GaInP window layer/stopetch layer and a GaAs contact layer. The heterojunction device includes a 3-µm-thick GaAs optical filter above the junction intended to minimize misleading photoresponse from the GaAs emitter layer. The structures were processed into solar cells with electroplated Au front grids and back contacts, with etched mesas defining an illuminated area of 0.10 cm^2. No antireflection coatings were applied. Several devices were fabricated on each wafer, and are designated, for example, as PA280#7.

3. DEVICE MEASUREMENT

To measure the current-voltage (IV) curves for the devices, the device currents were determined by integrating the measured external QEs of the devices against the ASTM standard AM1.5 Direct spectrum (1000 W/m^2) over the energy range below the GaAs band gap, since in the intended application in a multijunction device, the spectrum reaching the 1-eV cell will be filtered by the GaAs cell above it. The devices were then placed in the solar simulator and covered by a GaAs filter to remove light above the GaAs band edge. The simulator intensity was adjusted to set the short-circuit current of the device being measured in the simulator equal to its AM1.5D current calculated as described above. The IV curves were then measured at this simulator intensity. This approach assumes that the QE curves measured under low illumination accurately represent the QE under white light bias. We checked this assumption for device PA280#7 for light biases up to ~200mA/cm^2 and found that for photon energies below the GaAs band gap, the variation of QE with light bias is less than ±2%.

It should be emphasized that correctly measuring the IV curves for devices such as these, which are designed for operation under the spectral range of 1.0 to 1.4 eV, is not trivial. Before settling on the measurement technique described in the previous paragraph, we first tried measuring the IV curves by using a silicon reference cell calibrated while covered with a GaAs wafer to cut off the reference cell's photoresponse above the 1.4-eV GaAs band edge. One might at first expect such a reference cell setup to have a spectral response sufficiently similar to that of the GaInNAs devices under test to yield acceptably precise measurements of the photocurrents. However, this procedure generated spectral mismatch factors that differed from the ideal value of unity by almost a factor of two. There are at least three causes for this difficulty: (1) the

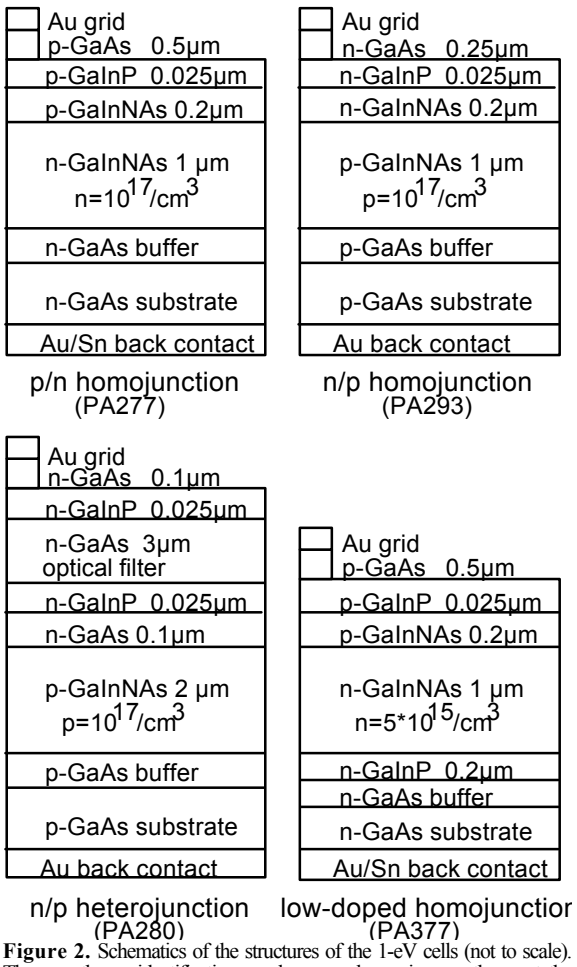

Figure 2. Schematics of the structures of the 1-eV cells (not to scale). The growth run identification numbers are shown in parentheses at the bottom of the figure. For each growth run, several devices were fabricated on the wafer, and are designated, for example, as PA280#7 in the tables and figures below.

spectral range of 1-1.4 eV is very narrow, (2) the spectrum of the simulator's xenon lamp has multiple spikes in this spectral region, and (3) for terrestrial spectra, there are two large atmospheric-absorption notches in the 1.0-1.4 eV spectral range. In addition, variations in the band gap of the GaInNAs alloy and drifts in the spectrum of the simulator can cause significant variation in the spectral correction factor, necessitating its measurement for every sample. We conclude that attempts to measure the currents for these devices by using the conventional expedient of a reference cell are likely to result in significant errors if a xenon arc lamp is the light source.

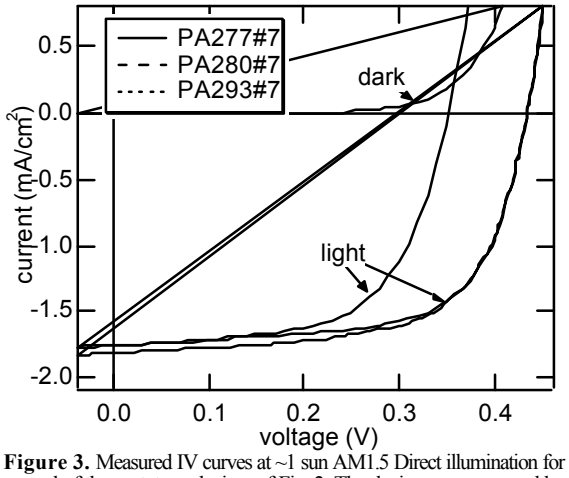

Figure 3. Measured IV curves at ~1 sun AM1.5 Direct illumination for several of the prototype devices of Fig. 2. The devices were covered by a GaAs filter and the currents were calibrated as described in the text. The corresponding dark IV curve for PA280#7 is shown also.

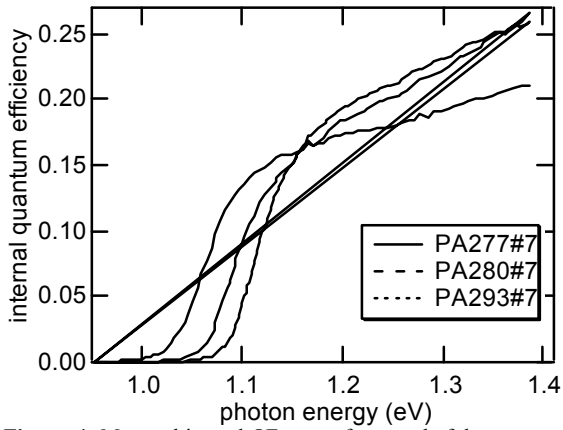

Figure 4. Measured internal QE curves for several of the prototype devices of Fig. 2.

Table II. GaAs-filtered AM1.5D device performance parameters V_{oc}, J_{sc}, and FF from the IV curves of Figs. 3 and 6(a); band gaps E_g from the QE curves of Figs. 4 and 6(b); and, in the last two columns, the currents calculated from the internal QE for the AM1.5D and AM0 solar spectra.

Device	V_{oc} (mV)	J_{sc} (mA/cm^2) ext. QE AM1.5D	FF (%)	E_g (eV)	J_{sc} (mA/cm^2) int.QE AM1.5D	J_{sc} (mA/cm^2) int. QE AM0
PA277#7	353	1.8	61	1.052	2.5	2.7
PA280#7	435	1.8	66	1.078	2.6	2.7
PA293#7	435	1.8	64	1.095	2.6	2.7
PA377#3	294	6.5	59	1.025	9.2	10.2

4. CONVENTIONAL PROTOTYPES: RESULTS

The short-circuit current (J_{sc}), open-circuit voltage (V_{oc}), and fill factor (FF) from these IV curves are summarized in Table II (the parameters for device PA377#3 will be discussed below). The IV curves are shown in Fig. 3. The corresponding dark-IV curve for the n/p heterojunction device, PA280, is shown also. A comparison of the light and dark IV curves for this device shows that the apparent shunt resistance visible in the light IV curve can be attributed to field-aided collection, as the dark IV curve is not shunted. The V_{oc} expected for an ideal device in this band-gap range would be ~0.6-0.7 V, so that the V_{oc} of the prototypes are within ~0.2 V of the ideal. The nonideality of the FFs appears to result from various causes including field-aided collection and the low J_{sc}, which is at least a factor of three less than expected. The problems with J_{sc} will be discussed below.

The crucial test of whether the devices convert photons down to the desired energy of 1 eV is whether the devices show photoresponse down to these energies. Figure 4 shows the measured internal QE curves for the devices whose IV curves are shown in Fig. 3. All device QE data presented in this paper were taken at short circuit, i.e., zero applied voltage bias, at very low light levels of $< 10^{-2}$ suns. The band edges, tabulated in Table II, are roughly 1 eV, as desired for the third junction in the three- or four-junction ultrahigh-efficiency device designs of Fig. 1. However, while the QE curves confirm the devices' conversion of light down to ~1 eV, the curves also indicate a serious deficiency in these devices: the QEs are a factor of 3–5 lower than the near-unity QE for a good-quality GaAs cell, resulting in the low J_{sc} values measured from the IV curves for these devices.

5. CONVENTIONAL PROTOTYPES: DISCUSSION

In order to study the QE problem in more detail, a series of GaInNAs epilayers were grown on GaAs substrates under a wide range of growth conditions, at various thicknesses, both without and with back-surface

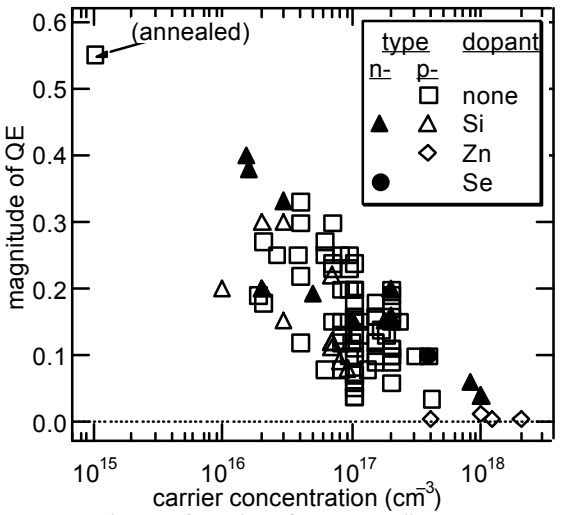

Figure 5. The QE of a variety of GaInNAs epilayers at 200 meV above the band edge, as a function of carrier concentration. All data shown are from layers with band gaps E_g<1.15 eV.

passivation layers, both without and with distillation purification of the DMHy source, and over a range of n- and p-type doping levels from $<10^{16}$/cm^3 to $>10^{18}$/cm^3. Growth temperatures from 550°C to 650°C, rates from 2.4μm/h to 7 μm/h, AsH_3/group-III ratios from 2 to 40, and DMHy/AsH_3 ratios from 7 to 100 were used. The as-grown epilayers were brought into contact with a liquid electrolyte, and the QEs of the resulting Schottky-barrier-like junctions were measured. The study is discussed in detail elsewhere [10]. The central finding is that the minority-carrier diffusion lengths are very short: shorter than the 0.04μm-0.4μm depletion widths. Thus there is carrier collection only from the depletion region. This is the cause of the field-aided collection behavior observable in the IV curves as noted above. Figure 5 shows the magnitude of the QE for a number of epilayers grown under a wide range of growth conditions as a function of the carrier concentration. The QE is seen to be determined by the carrier concentration, because of the dependence of the carrier concentration on the depletion width.

It remains to be determined whether the short diffusion lengths are due to extrinsic/ growth-related defects or instead to characteristics intrinsic to the GaInNAs material. A possible cause of extrinsic defects might be impurities introduced from an insufficiently pure DMHy source. Intrinsic causes of the short diffusion lengths might include localized energy states in the band structure [11], or spatially localized band fluctuations resulting from GaN clustering. If the cause of the short diffusion lengths is extrinsic, it should in principle be possible with further development to grow GaInNAs with a photoresponse comparable to that of good-quality GaAs. In this case, extension of the GaInP/GaAs two-junction device to three and four junctions by addition of a GaInNAs junction, as illustrated in Fig. 1, would result in the achievement of the efficiency boosts of Table I. If, however, the diffusion-length problem is an intrinsic one, the efficiency boosts of Table I will not be achievable with the GaInNAs device. Work on determining the cause of the low diffusion lengths is under way.

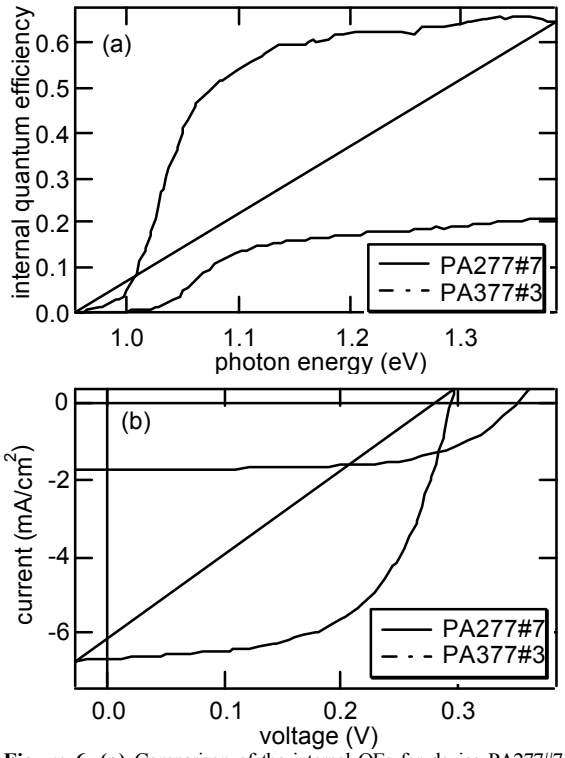

Figure 6. (a) Comparison of the internal QEs for device PA277#7, which has an n=10^{17}/cm^3 conventionally-doped base, and device PA377#3, which has an n=5∞10^{15}/cm^3 lightly-doped base. **(b)** Comparison of the IV curves for PA277#7 and PA377#3. Curves were measured as for Fig. 3.

6. ENHANCED-DEPLETION-WIDTH DEVICE: RESULTS AND DISCUSSION

In order to study the effect of the depletion width on the photocurrent in a full device structure, we fabricated a p/n homojunction device, PA377 in Fig. 2, whose main difference from the device PA277 is a much lower base doping of $n \approx 5\infty10^{15}$/cm^3 than the $n \approx 1\infty10^{17}$/cm^3 doping of PA277, as measured by capacitance-voltage (CV) measurement. The corresponding depletion width for PA377 as measured by CV is ~0.5 μm, a significant fraction of the 1-μm base layer thickness, and much greater than the 0.1-μm depletion width for the higher-doped PA277. The QEs for the two devices are compared in Fig. 6(a). The lower doping and consequent greater depletion width of PA377 give a significantly enhanced QE compared with PA277. Figure 6(b) compares the IV curves for these two devices. The enhanced QE for PA377 is reflected in a correspondingly enhanced J_{sc}. The overall efficiency of the device is not proportionally enhanced, because the V_{oc} is diminished, mostly because of the increased dark current. (Additionally, 30 to 70 mV of the decreased V_{oc}, and a small fraction of the increased J_{sc}, are due to the lower band gap for PA377 than for the other devices, as listed in Table II.) The dark currents for the devices discussed here are shown in Fig. 7, with lines corresponding to ideality factor n=1 and n=2 dark currents included for comparison. While PA293 has n=2, all the other devices have roughly n≈1.5. The Sah-Noyce-Shockley treatment [12] of recombination/ generation currents in the depletion region gives n ranging from n≈1 for shallow recombination centers to n≈1.8 for deep centers. Therefore the n≈1.5 ideality factors of Fig. 7 suggest that these devices may have trap levels intermediate between deep and shallow.

The tradeoff of increased current at the expense of

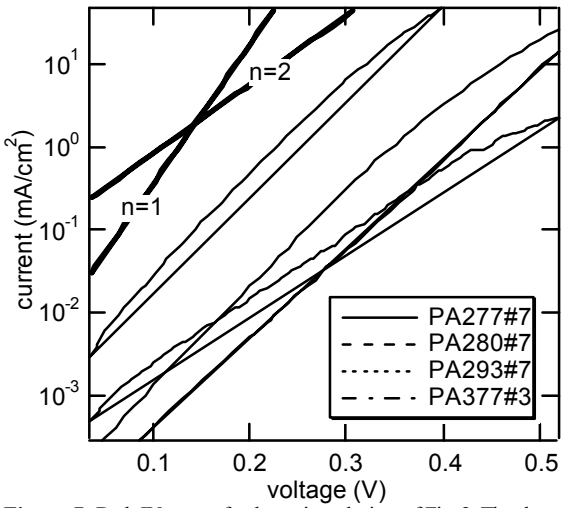

Figure 7. Dark IV curves for the various devices of Fig. 2. The slopes corresponding to ideality factors n=1 and 2 are indicated by the thick dotted lines labeled "n=1" and "n=2".

decreased voltage may make it possible to meet the current-matching requirements for the third cell of the series-connected three- and four-junction devices of Fig. 1. A current of ~14 mA/cm^2 would be required from the GaInNAs device for current matching. Table II lists for each device the results of a calculation of the J_{sc} for the AM1.5D spectrum using the *internal* QEs of the devices, which is a reasonable projection of what the J_{sc} would be if high-quality antireflection coatings were applied to the devices. Device PA377#3 has a projected current of 9.2 mA/cm^2, which is within a factor of two of the current required for current-matching [1]. Bringing the current of future devices up to the current-matching value may be possible but will be challenging, because to achieve a sufficiently large depletion depth to bring the photocurrent up enough for current-matching would require a base doping density on the order of $1\infty10^{15}$/cm^3. Achieving such a low doping density will not be easy given the $p\approx1\infty10^{17}$/cm^3 background doping, requiring either a very delicate *n*-type counter-doping, a change in a growth condition (e.g., switching from dimethylhydrazine to an alternate source such as tertiarybutylhydrazine or plasma-cracked N_2) so as to reduce the background doping, or a treatment such as annealing [10] to lower the background doping level. The difficulty is illustrated by the variation in doping density which occurred across the PA377 wafer. Although only the #3 device from the wafer is discussed in this paper in detail, a total of a dozen devices were fabricated on the wafer. Doping densities on the various PA377 devices varied from the $n=5\infty10^{15}$/cm^3 of #3 to an order of magnitude higher, with corresponding depletion widths and photocurrents lower by a factor of 2 or more. Thus, it may be possible to use this high-depletion-width low-voltage/enhanced-current version of the GaInNAs device as the third cell to gain an efficiency boost over the two-junction device, if the challenges associated with low base doping can be overcome. Alternatively to the low-doping approach, it might be possible to improve current collection by using a graded-band-gap or graded-doping base. It should be kept in mind that if it does prove possible to improve current collection enough to achieve current-matching and allow use of the GaInNAs device in the three- and four-junction devices of Fig. 1, the tradeoff of decreased V_{oc} for increased current means that the efficiency benefits of the GaInNAs third junction will be less than expected from the idealized calculations summarized in Table I. In order to model the device performance accurately enough to make a more precise statement about the effect of the decreased V_{oc}, it will be necessary to make measurements of GaInNAs materials parameters such as lifetimes and effective masses for which limited or no data exists for this new materials system.

7. CONCLUSIONS

Prototype solar cells with GaInNAs active layers have demonstrated photoresponse down to the 1-eV photon energy required for the third junction of future-generation multijunction devices. The internal QEs for devices with standard base dopings of 10^{17}/cm^3 are very low, on the order of 0.2, because of the low minority-carrier diffusion lengths in the GaInNAs layer. Efforts to understand and eliminate the cause of the low diffusion lengths are ongoing. Lowering the base doping greatly improves the photocurrent at the expense of the voltage and fill factor by increasing the depletion width. If challenges associated with the low doping can be met, it might be possible to use such a field-enhanced device in the multijunction structures of Fig. 1, although the efficiency benefits would be less than predicted in Table I.

ACKNOWLEDGMENTS

This work was supported by the U.S. Department of Energy contract number DE-AC36-83CH10093. We thank C. Kramer for help with the device fabrication, H. Field for help with device-measurement issues, and R. Reedy for SIMS measurements.

REFERENCES

[1] K.A. Bertness, S.R. Kurtz, D.J. Friedman, A.E. Kibbler, C. Kramer, and J.M. Olson, Appl. Phys. Lett. **65** (1994) 989.

[2] S.R. Kurtz, K.A. Bertness, D.J. Friedman, A.E. Kibbler, C. Kramer, and J.M. Olson, 1st World Conference on Photovoltaic Energy Conversion (1994) 2108.

[3] D.J. Friedman, S.R. Kurtz, K.A. Bertness, A.E. Kibbler, C. Kramer, and J.M. Olson, Progr. Photovolt. **3** (1995) 47.

[4] T. Takamoto, E. Ikeda, H. Kurita, and M. Ohmori, Appl. Phys. Lett. **70** (1997) 381.

[5] P.K. Chiang, J.H. Ermer, W.T. Nishikawa, D.D. Krut, D.E. Joslin, J.W. Eldredge, B.T. Cavicchi, and J.M. Olson, 25th IEEE Photovoltaic Specialists Conference (1996) 183.

[6] S.R. Kurtz, D. Myers, and J.M. Olson, 26th IEEE Photovoltaic Specialists Conference (1997) 875.

[7] M. Weyers, M. Sato, and H. Ando, Jpn. J. Appl. Phys. **31** (1992) 853.

[8] M. Kondow, K. Uomi, A. Niwa, T. Kitatani, S. Watahiki, and Y. Yazawa, Jpn. J. Appl. Phys. **35** (1996) 1273.

[9] M. Weyers and M. Sato, Appl. Phys. Lett **62** (1993) 1396.

[10] J.F. Geisz, D.J. Friedman, J.M. Olson, S.R. Kurtz, and B.M. Keyes, J. Cryst. Gr. (in press)

[11] L. Bellaiche, S.-H. Wei, and A. Zunger, Phys. Rev. B **56** (1997) 10233.

[12] C.T. Sah, R.N. Noyce, and W. Shockley, Proc. IRE **45** (1957) 1228.